Journal of Geophysical Research: Biogeosciences

RESEARCH ARTICLE
10.1029/2017JG004248

Upwelling of Macronutrients and Dissolved Inorganic Carbon by a Subglacial Freshwater Driven Plume in Bowdoin Fjord, Northwestern Greenland

Naoya Kanna[1], Shin Sugiyama[1,2], Yoshihiko Ohashi[2,3], Daiki Sakakibara[1], Yasushi Fukamachi[1,2,4], and Daiki Nomura[1,5]

[1]Arctic Research Center, Hokkaido University, Sapporo, Hokkaido, Japan, [2]Institute of Low Temperature Science, Hokkaido University, Sapporo, Hokkaido, Japan, [3]Graduate School of Environmental Science, Hokkaido University, Sapporo, Hokkaido, Japan, [4]Global Station for Arctic Research, Global Institution for Collaborative Research and Education, Hokkaido University, Sapporo, Hokkaido, Japan, [5]Faculty of Fisheries Sciences, Hokkaido University, Hakodate, Hokkaido, Japan

Key Points:
- Nutrient transport by a subglacial discharge plume was quantified in Greenland
- Nutrient-rich deep fjord water accounted for >80% of the upwelling plume water
- Summer phytoplankton blooms in the fjord were driven by plume nutrient transport

Supporting Information:
- Supporting Information S1
- Data Set S1
- Data Set S2

Correspondence to:
N. Kanna,
kanna@arc.hokudai.ac.jp

Citation:
Kanna, N., Sugiyama, S., Ohashi, Y., Sakakibara, D., Fukamachi, Y., & Nomura, D. (2018). Upwelling of macronutrients and dissolved inorganic carbon by a subglacial freshwater driven plume in Bowdoin Fjord, northwestern Greenland. *Journal of Geophysical Research: Biogeosciences*, *123*, 1666–1682. https://doi.org/10.1029/2017JG004248

Received 23 OCT 2017
Accepted 22 APR 2018
Accepted article online 1 MAY 2018
Published online 23 MAY 2018

Abstract In Greenland, tidewater glaciers discharge turbid subglacial freshwater into fjords, forming a plume near the calving front. To elucidate the effects of this discharge on nutrient and dissolved inorganic carbon transport to the surface in these fjords, we conducted observational studies on Bowdoin Glacier and in its fjord in northwestern Greenland during the summer of 2016. Our results provide evidence of macronutrient and dissolved inorganic carbon transport from deep in the fjord to the surface in front of the glacier. This transport is driven by plume formation resulting from subglacial freshwater discharge and subsequent upwelling along the glacier calving front. The plume water is a mixture of subglacial freshwater and entrained fjord water. The fraction of glacial meltwater in the plume water is ~14% when it reaches the surface. The plume water is highly turbid because it contains substantial amounts of sediment derived from subglacial weathering. After reaching the surface, the plume water submerges and forms a turbid subsurface layer below fresher surface water at densities of 25.0 to 26.5 σ_θ. Phytoplankton blooms (~6.5 μg/L chlorophyll *a*) were observed near the boundary between the fresher surface and turbid subsurface layers. The bloom was associated with a strong upward $NO_3^- + NO_2^-$ flux, which was caused by the subduction of plume water. Our study demonstrated that the subglacial discharge and plume formation at the front of Bowdoin Glacier play a key role in the availability of nutrients and the subsequent growth of phytoplankton in the glaciated fjord.

1. Introduction

The Greenland Ice Sheet drains freshwater into the ocean through land- and marine-terminating outlet glaciers. The discharge from the glaciers plays critical roles in coastal marine environments as well as the ice sheet mass budget. For example, glacial discharge carries substantial amounts of suspended sediment (SS) from glacial erosion, affecting the water properties and depositional conditions in the ocean (Chu et al., 2012; Ohashi et al., 2016; Overeem et al., 2017). From the land-terminating glaciers, sediment-laden meltwater enters the ocean through proglacial streams and lakes. The turbid meltwater spreads and covers the ocean surface over an area extending several kilometers, which is observable in satellite images (Chu et al., 2012; Hopwood et al., 2015; Ohashi et al., 2016). From the marine-terminating outlet glaciers, sediment-laden subglacial freshwater is typically released at depths of up to several hundred meters. The subglacial discharge upwells along the calving front to form a buoyant plume, and plume water reaches near the surface of fjords (Chu, 2014; Mankoff et al., 2016). The percentage of the area covered by marine-terminating outlet glaciers has been reported as 34.9% of Greenland (Gardner et al., 2013); thus, the corresponding discharge is a key driver of the fjord-scale water column structure and properties of the coastal environments around Greenland.

Meire et al. (2017) have reported that phytoplankton productivity is regulated quite differently in fjords influenced by either marine-terminating or land-terminating glaciers. Phytoplankton are important primary producers, as they ensure a crucial energy supply to higher trophic animals within fjords. In addition to favorable light conditions, phytoplankton require macronutrients (nitrate, phosphate, and silicate), micronutrients (e.g., iron), and dissolved inorganic carbon (DIC) for their growth. Glacier discharge can either dilute or enhance the concentrations of these biogeochemical components within the surface layer of fjords

(Fransson et al., 2015; Hopwood et al., 2016; Meire et al., 2016). Upwelling of a turbid subglacial discharge plume (hereafter, plume) originating from marine-terminating outlet glaciers entrains nutrient-rich deep water, which sustains high productivity throughout summer in fjords (Meire et al., 2017). However, a fjord with only land-terminating glaciers lacks this upwelling mechanism and is characterized by lower productivity (Meire et al., 2017). The region influenced by the plume near the calving front of marine-terminating outlet glaciers has also been recognized as an important foraging hotspot for higher trophic animals, which include seabirds and marine mammals (Lydersen et al., 2014; Urbanski et al., 2017). Therefore, discharge from marine-terminating outlet glaciers plays an important role in the productivity of fjord ecosystems by affecting nutrient availability for primary producers (e.g., Meire et al., 2017) and subsequent production of zooplankton, which comprises a vital link between primary production and the higher trophic animals. Several studies have performed comprehensive observations of the nutrient delivery associated with meltwater inputs (Hawkings et al., 2015, 2017; Hopwood et al., 2016; Meire et al., 2016; Wadham et al., 2016). However, processes associated with macronutrient supply to surface waters via plumes are not quantitatively understood.

In this study, we present measurements of the biogeochemical components of water directly sampled from a buoyant plume in front of Bowdoin Glacier, a marine-terminating outlet glacier in northwestern Greenland. We also report hydrographic and biogeochemical data obtained from the glacier and its fjord. By combining these data, we provide quantitative interpretations of nutrient and DIC transport to surface waters by the plume and discuss its effect on the distribution of phytoplankton.

2. Materials and Methods

2.1. Observation Sites

Field observations were conducted on Bowdoin Glacier between 4 and 21 July 2016 and in Bowdoin Fjord on 27 and 29 July 2016 (Figure 1a). Bowdoin Glacier is a marine-terminating outlet glacier in northwestern Greenland that discharges freshwater into Bowdoin Fjord through a 3-km-wide calving front. The ice thickness is approximately 250–400 m within 6 km of the terminus, and 86–89% of the entire ice thickness of the terminus is situated below sea level (Sugiyama et al., 2015). The glacier terminus is grounded (see Figure 4 in Sugiyama et al., 2015), and hence, the terminus is not likely to have a floating tongue. The 4-km-wide land-terminating Tugto Glacier flows several kilometers west of Bowdoin Glacier (Tsutaki et al., 2016), and its proglacial stream feeds the fjord ~1 km from the calving front of Bowdoin Glacier (Figures 1a and 1b). Bowdoin Fjord is approximately 20 km long and is covered with sea ice, typically until early July. During our study period, a persistent patch of sediment-rich waters was observed at the fjord surface in front of Bowdoin Glacier. We interpret this patch as a plume characterized by turbid flow visibly rising toward the fjord surface near the calving front. This sea-ice-free and highly turbid zone is maintained by upwelling subglacial discharge (Figures 1c and 1d). In the summer of 2016, sea ice began retreating in mid-July and disappeared from the fjord by the end of July.

2.2. Sampling and Sample Preparation

Coordinates of the main sampling stations are available in Dataset S1 of the supporting information. Supraglacial meltwater samples were collected by hand directly into 2-L high-density polyethylene bottles at eight stations (Sts. G, Figure 1a); each sample was then divided into several subsamples. Water samples near a proglacial stream (salinity < 3), which flows on the eastern side of Bowdoin Glacier, were collected at the three stations on a beach near the eastern side of the calving front (Sts. R, Figure 1b). For macronutrient analysis, water samples were transferred into 10-ml acrylic tubes without filtration. For DIC analysis, samples were placed into 120-ml glass vials. A saturated $HgCl_2$ solution (Wako Pure Chemical Industries, Ltd., Japan) was added to the samples for macronutrient (Kattner, 1999) and DIC analysis to avoid biological activity. Subsamples for salinity and oxygen isotopic composition ($\delta^{18}O$) analyses were collected into glass bottles with rubber inserts in the caps. For chlorophyll *a* (Chl *a*) analysis, water samples of 100–200 ml were filtered through 25 mm GF/F filters (Whatman, USA) under gentle vacuum (<0.013 MPa). The Chl *a* on the filter was extracted in *N*,*N*-dimethylformamide (Wako Pure Chemical Industries, Ltd.) for 24 hr in the dark (Suzuki & Ishimaru, 1990). SS for particulate organic matter (POM) analysis was collected onto precombusted (450°C for 5 hr) 47-mm GF/F filters (Whatman, USA) and then wrapped with precombusted aluminum foil before being transferred to Petri dishes. Water volumes needed for the filtration are summarized in Dataset S1.

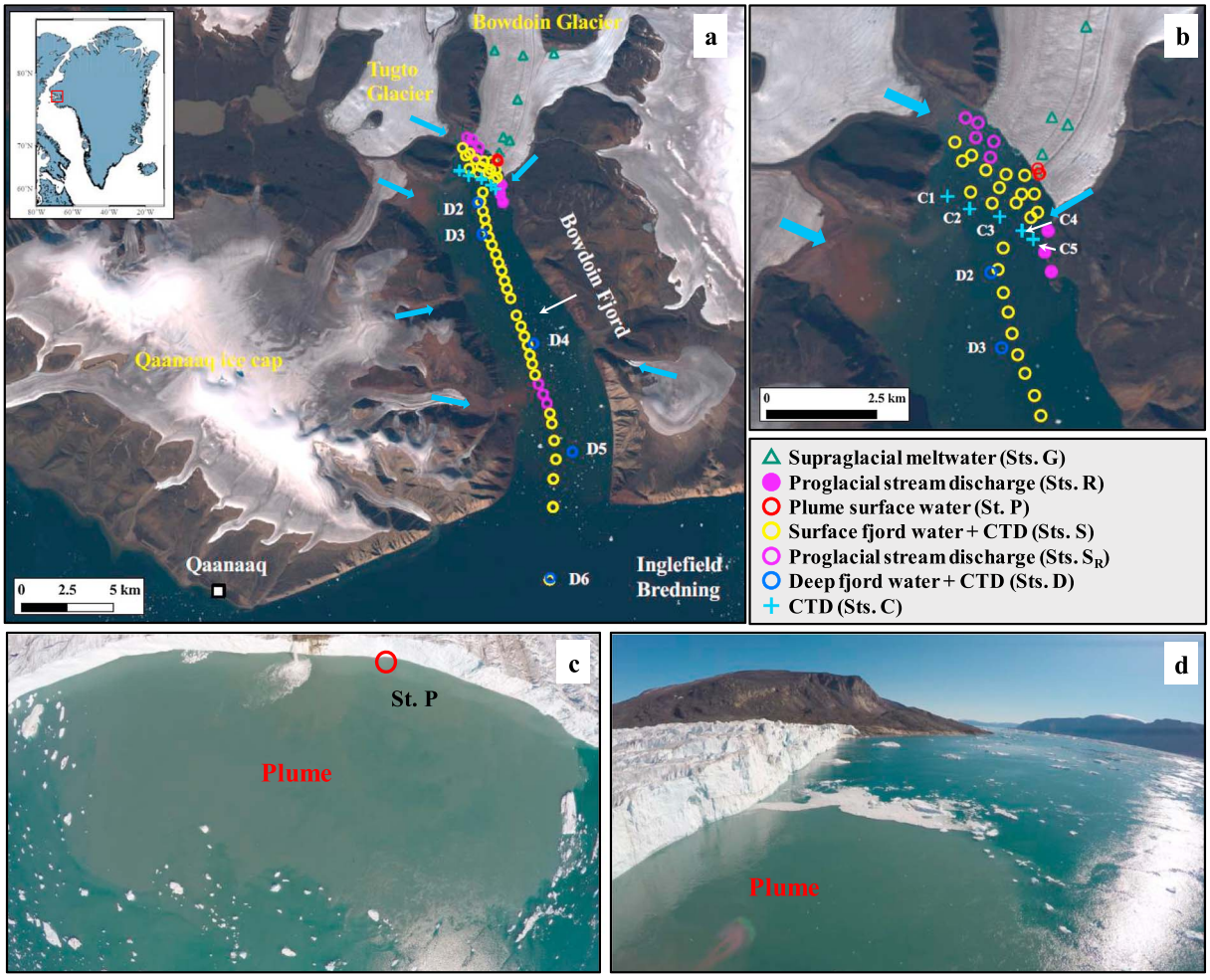

Figure 1. (a) Landsat image (acquired on 30 July 2016) of Bowdoin Glacier and its fjord, showing the sampling locations of supraglacial meltwater, proglacial stream discharge, plume surface water, surface fjord water, and deep fjord water. The inset shows the location of the study site in northwestern Greenland. The blue arrows indicate the proglacial stream discharge. (b) Study area near the calving front of Bowdoin Glacier. (c and d) Photographs of a plume (acquired 16 July 2016) taken from an unmanned aerial vehicle, courtesy of G. Jouvet, Y. Weidmann, and J. Seguinot, ETH Zürich. CTD = conductivity-temperature-depth.

Water sampling at the plume surface was performed four times on 8, 10, 15, and 16 July 2016 (St. P, Figures 1 and S1). These samples were collected from the edge of the glacier front, by lowering 500-ml polycarbonate bottles using a fishing rod and string. The plume samples were divided into subsamples for the macronutrients, DIC, salinity, $\delta^{18}O$ analyses without filtration, and for Chl *a* and POM analyses, in which the same procedures described above were applied. Because immediate preservation of the samples in a freezer was logistically difficult, the subsamples for macronutrient, Chl *a* (extracted in *N*,*N*-dimethylformamide), and POM analyses were preserved with ice in an insulated container for 2 weeks during our field campaign on the glacier. Immediately after our return from the glacier, these subsamples were placed in a freezer (−15°C) and transported to Japan at −15°C. The samples were stored in a cold laboratory (−20°C) until they were analyzed for Chl *a*, macronutrients, and POM for 1, 2, and 7 months after sample collection, respectively. Note that the degradation of these samples between collection and analysis was not likely to have occurred based on our additional tests, which are shown in Table S1 and Dataset S2.

Surface fjord water sampling and hydrographic data collection were conducted using a 5-m-long boat from within 1 km of the calving front of Bowdoin Glacier to the outer area of Bowdoin Fjord on 27 July 2016 (Figure 1a). A conductivity-temperature-depth profiler equipped with turbidity, fluorescence, and fast-responding dissolved oxygen sensors (model: ASTD 102, JFE Advantech, Japan) was mounted on a pole and hung from the side of the boat to perform continuous measurements of turbidity and temperature in the surface waters (0.3 m depth). Additionally, 49 surface water samples were collected by hand at 0 m

and placed directly into 2-L high-density polyethylene bottles from the side of the boat (Sts. S). Samples collected from highly turbid areas (> 8 FTU) were defined as proglacial stream discharge, which we regarded as a subglacial meltwater proxy from a land-terminating glacier (Sts. S_R).

Hydrographic measurements were also conducted on 29 July 2016 at five locations (Sts. C1–5) along a survey line across the fjord 1.3 km off the calving front and at an additional five locations (Sts. D2–6) along the centerline of the fjord (Figure 1a). The conductivity-temperature-depth profiler used for the deep measurement was hung from a Kevlar rope and lowered into the water to measure the water properties (conductivity, temperature, water pressure, turbidity, fluorescence, and dissolved oxygen) every 1 s (~1-m intervals). Apparent oxygen utilization (AOU) was calculated based on the measured dissolved oxygen and water salinity, temperature, and pressure as per Benson and Krause (1984). Fjord water was sampled at Sts. D2–6 along the fjord's centerline at depths of 0–760 m with a Niskin sampler (model: 1010, General Oceanics Inc., USA) suspended on a Kevlar rope using messengers to close the sampler. All collected seawater samples were divided into subsamples for macronutrient, DIC, salinity, $\delta^{18}O$, Chl *a*, and POM analyses after returning from the fjord. After sample processing, the subsamples for macronutrient, Chl *a* (extracted in *N*,*N*-dimethylformamide), and POM analyses were immediately placed in a freezer (−15°C), transported to Japan at −15°C, and then stored in a cold laboratory (−20°C) until their analyses. The salinity and Chl *a* obtained from the sample analyses were used to calibrate salinity and fluorescence from the conductivity-temperature-depth profiler, respectively.

2.3. Sample Analyses

Macronutrients ($NO_3^- + NO_2^-$, PO_4^{3-}, and $Si(OH)_4$) were measured using an autoanalyzer (QuAAtro, BL TEC Inc., Japan) with a continuous flow system. Samples were filtered before analysis using syringe GF/F filters (Whatman, USA). The macronutrients in the GF/F filter blanks were undetectable with our method (data not shown). Quality control was carried out using a reference material (KANSO Technos Co., Ltd, Japan) consisting of 18.60 ± 0.057 μmol/L $NO_3^- + NO_2^-$, 0.483 ± 0.0034 μmol/L NO_2^-, 1.328 ± 0.007 μmol/L PO_4^{3-}, and 43.07 ± 0.22 μmol/L $Si(OH)_4$. The reference material concentrations measured with our methods (N = 15, 18.99 ± 0.29 μmol/L $NO_3^- + NO_2^-$, 0.500 ± 0.008 μmol/L NO_2^-, 1.274 ± 0.027 μmol/L PO_4^{3-}, and 43.55 ± 0.79 μmol/L $Si(OH)_4$ with a seawater density of 1.025 kg/L) agreed well with the certified values.

The DIC concentrations were determined by the coulometric technique reported by Johnson et al. (1985). The DIC measurement was calibrated with reference seawater materials (Batch AG; KANSO Technos Co., Ltd, Japan), which is traceable to the Certified Reference Material distributed by A. G. Dickson (Scripps Institution of Oceanography, La Jolla, CA, USA). The standard deviation obtained by repeated measurements of a reference seawater material (N = 20, DIC = 2085 μmol/L) was 1.4 μmol/L.

The salinity of the fjord water was determined with a salinometer (AUTOSAL 8400B, Guildline Instruments, USA; instrumental accuracy: <0.002). To determine the salinity of supraglacial and plume surface water, chloride concentrations were determined with a salt/chloride analyzer (Model SAT-500, Towa Electronic Industry, Japan; our analytical precision: ±0.05) and converted to salinity using a calibration curve determined by paired salinity (determined with an AUTOSAL 8400B salinometer) and chloride measurements.

$\delta^{18}O$ values were determined with a mass spectrometer (DELTA plus, Finnigan MAT). The analytical precision was estimated to be <0.05‰ from the root mean square of the differences between measurements repeated twice.

Chl *a* concentrations were determined with a fluorometer (10-AU, Turner Designs, USA) using the nonacidification method of Welshmeyer (1994) or a handheld fluorometer (AquaFluor, Turner Designs, USA).

For POM analysis, frozen SS samples on 47-mm GF/F filters were thawed and dried at +60°C before the weight of sediments on the filter was measured. Carbonate materials on the filter were removed by adding a few drops of 20% HCl (Wako Pure Chemical Industries, Ltd., Japan). After drying the samples for 2 days in a glass desiccator with NaOH pellets (Wako Pure Chemical Industries, Ltd., Japan) and P_2O_5 powder (Wako Pure Chemical Industries, Ltd., Japan), the particulate organic carbon (POC) and nitrogen (PON) contents were measured by processing 2-cm pieces of the filter using an elemental analyzer (Model NA-1500, Fisons Co. Ltd., USA). All data are available in Dataset S1 of the supporting information.

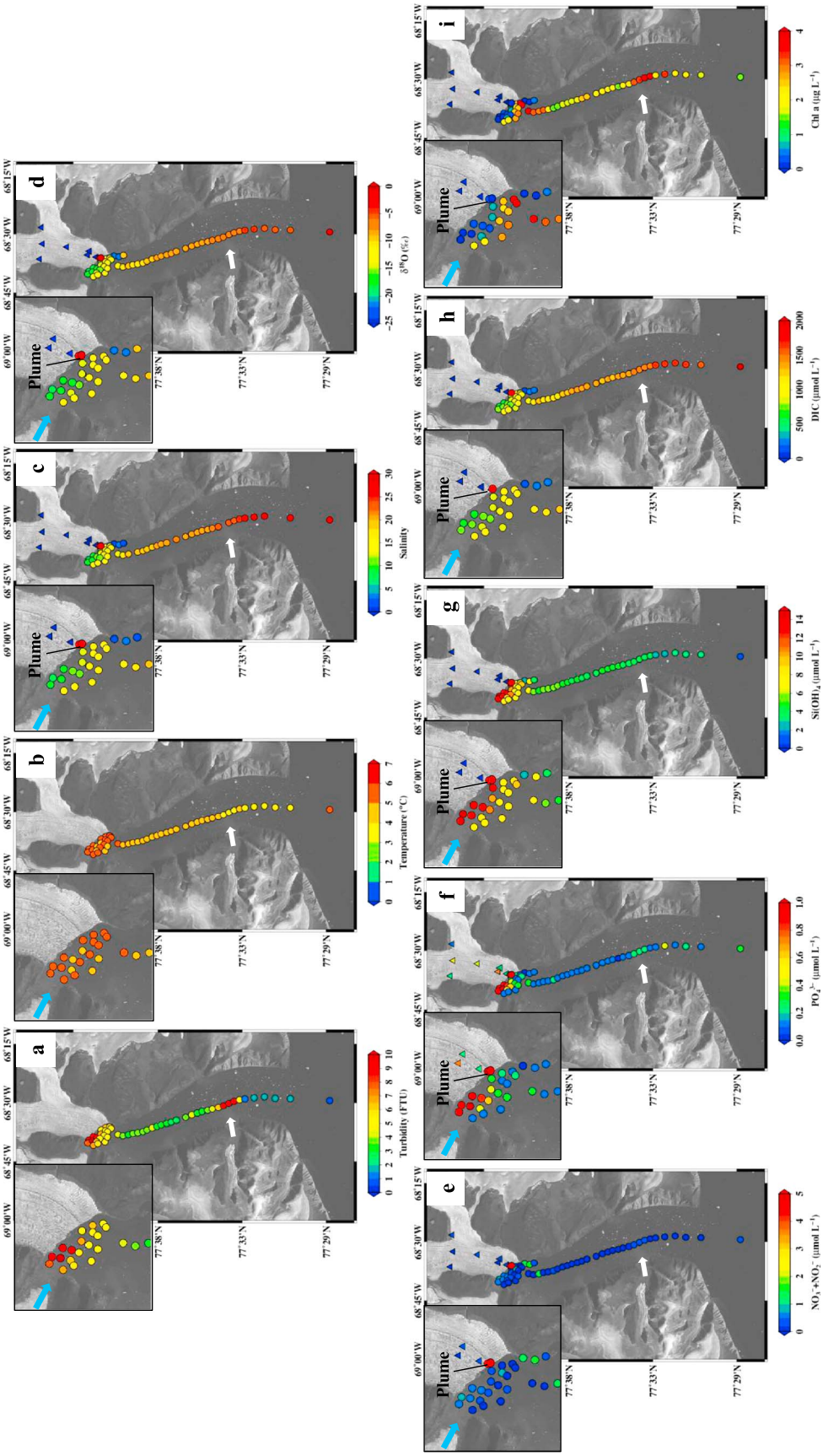

Figure 2. Spatial distributions of (a) turbidity, (b) temperature, (c) salinity, (d) $\delta^{18}O$, and concentrations of (e) $NO_3^- + NO_2^-$, (f) PO_4^{3-}, (g) $Si(OH)_4$, (h) dissolved inorganic carbon (DIC), and (i) chlorophyll *a* (Chl *a*) on Bowdoin Glacier and in its fjord. Data pertaining to supraglacial meltwater and fjord water (including proglacial stream discharge and plume surface water) are represented by triangles and circles, respectively. The inset shows data near the calving front of Bowdoin Glacier. The blue and white arrows indicate the water influenced by subglacial discharge throughout proglacial stream near land-terminating glacier.

Table 1
Values of the Average and Standard Deviation of Salinity, $\delta^{18}O$, and Concentrations of SS, POC, PON, DIC, Macronutrients, and Chl a in Supraglacial Meltwater, Proglacial Stream Discharge, Fjord Surface Water (Outside Plume) Within 1 km From the Calving Front (Sts. S1–15), and Plume Surface Water

Samples	Salinity	$\delta^{18}O$ (‰)	SS (mg/L)	POC (μmol/L)	PON (μmol/L)	DIC (μmol/L)	Macronutrient (μmol/L)			Chl *a* (μg/L)
							$NO_3^- + NO_2^-$	PO_4^{3-}	$Si(OH)_4$	
Supraglacial meltwater (Sts. G)	0 (*N* = 8)	−26.0 ± 0.4 (*N* = 8)	11.4 ± 9.3 (*N* = 7)	4.7 ± 1.5 (*N* = 7)	0.5 ± 0.2 (*N* = 7)	32.2 ± 6.0 (*N* = 8)	0.2 ± 0.2 (*N* = 8)	0.3 ± 0.2 (*N* = 8)	<DL (*N* = 8)	0.04 ± 0.04 (*N* = 8)
Proglacial stream discharge (Sts. R and S_R)	1.9 to 10.2 (*N* = 8)	−21.4 to −9.7 (*N* = 8)	9.8 to 42.1 (*N* = 3)	7.2 to 20.6 (*N* = 3)	0.8 to 1.9 (*N* = 3)	112 to 743 (*N* = 3)	0.2 to 1.6 (*N* = 8)	0.1 to 1.2 (*N* = 8)	2.3 to 15.1 (*N* = 8)	0.02 to 0.5 (*N* = 8)
Fjord surface water (Sts. S)	13.8 ± 1.2 (*N* = 14)	−13.5 ± 1.0 (*N* = 15)	21.0 ± 1.4 (*N* = 3)	27.3 ± 23.9 (*N* = 3)	4.0 ± 3.3 (*N* = 3)	921 ± 64 (*N* = 15)	0.2 ± 0.2 (*N* = 15)	0.2 ± 0.1 (*N* = 15)	8.1 ± 2.0 (*N* = 15)	2.8 ± 2.3 (*N* = 15)
Plume surface water (Sts. P)	31.2 ± 2.4 (*N* = 4)	−3.2 ± 1.8 (*N* = 4)	95.7, 132 (*N* = 2)	6.7, 28.4 (*N* = 2)	0.8, 2.3 (*N* = 2)	2059 (*N* = 1)	12.3 ± 0.6 (*N* = 4)	1.0 ± 0.1 (*N* = 4)	12.3 ± 0.7 (*N* = 4)	0.1 ± 0.1 (*N* = 3)

Note. Values of those in proglacial stream discharge are shown in ranges. *N* = number of samples; <DL = below limit of detection (<0.2 μmol/L); SS = suspended sediment; POC = particulate organic carbon; PON = particulate organic nitrogen; DIC = dissolved inorganic carbon; Chl *a* = chlorophyll *a*.

3. Results

3.1. Properties of Supraglacial Meltwater, Proglacial Stream Discharge, Fjord Surface Water, and Plume Surface Water

Figure 2 shows the spatial distributions of the physical and biogeochemical components of meltwater on Bowdoin Glacier and surface water in Bowdoin Fjord. In supraglacial meltwater, salinity and Chl *a* were near zero, the mean DIC concentration was 32.2 ± 6.0 μmol/L, and macronutrient concentrations were 0.2 ± 0.2 μmol/L $NO_3^- + NO_2^-$, 0.3 ± 0.2 μmol/L PO_4^{3-}, and below the limit of detection (<0.2 μmol/L) for $Si(OH)_4$ (Table 1). The values of $\delta^{18}O$ ranged from −26.5‰ to −25.1‰, with an average of −26.0 ± 0.4‰ (Table 1).

Near the calving front (within 1 km from the glacier terminus), surface water properties were substantially different from those in the other areas of the fjord. Turbidity generally increased, whereas salinity and $\delta^{18}O$ decreased toward the glacier terminus (Figures 2a, 2c, and 2d). Within the plume (St. P in Figure 1), surface water showed higher salinity (31.2 ± 2.4) and $\delta^{18}O$ (−3.2 ± 1.8‰) values and greater concentrations of macronutrients (12.3 ± 0.6 μmol/L $NO_3^- + NO_2^-$; 1.0 ± 0.1 μmol/L PO_4^{3-}; 12.3 ± 0.7 μmol/L $Si(OH)_4$) and DIC (2059 μmol/L; Table 1). The collected plume surface water contained high amounts of SS, which was up to 132 mg/L (Table 1). Interestingly, the concentration of Chl *a* was significantly lower in the plume (0.1 ± 0.1 μg/L; Table 1). High-turbidity (up to 17 FTU) and low-salinity (as low as 7.9) water were distributed in the fjord near the western side of the calving front, which was influenced by sediment-laden meltwater discharge from Tugto Glacier (indicated by blue arrow in Figures 2a and 2c). In this area, PO_4^{3-} (up to 1.2 μmol/L) and $Si(OH)_4$ (up to 14 μmol/L) concentrations were relatively high, whereas $\delta^{18}O$ was as low as −18.4‰ (Figures 2d, 2f, and 2g). The Chl *a* concentration in this area was also lower (as low as 0.1 μg/L) than that in the region >1 km from the glacier (>1 μg/L; Figure 2i). We also observed a patch of highly turbid water (up to 15 FTU) with a high Chl *a* concentration (>4 μg/L) at 77°33′N, which was likely influenced by glacial meltwater inputs (indicated by white arrow in Figures 2a and 2i).

Figures 3a and 3b show relationships between Chl *a* and POM concentrations in the supraglacial meltwater, proglacial stream discharge, fjord water, and plume surface water. POC and PON concentrations were positively correlated with Chl *a* (Pearson correlation coefficients $R = 0.82$, $p < 0.01$). The POC to PON ratios (C/N) in the fjord water were within the range of 5.1 to 7.1, regardless of POC concentrations, except for the relatively large values (8.1–10.8) obtained in the region influenced by the proglacial stream discharge (Figure 3c). Compared with the fjord water, samples collected from the plume surface water (8.6–12.2) and the supraglacial meltwater (7.8–12.8) showed significantly higher C/N ratios (Wilcoxon rank-sum test, $p < 0.01$).

3.2. Vertical Distributions of Physical and Biogeochemical Parameters in Fjord Water

Figures 4 and 5 show water properties within vertical cross section across the fjord 1.3 km off the calving front (Sts. C1–5) and along the centerline of the fjord (Sts. C3 and D2–6), respectively. According to the potential temperature (P-temperature)-salinity diagrams along these cross sections (Figure 6), water properties in Bowdoin Fjord were characterized by a mixture of cold and fresh Arctic-origin water (polar water [PW]) and relatively warm and saline Atlantic-origin water (Atlantic water [AW]; Beaird et al., 2015; Straneo et al., 2012).

At 1.3 km off the calving front, the range of high-turbidity water (hereafter, subsurface plume water) was distributed over a subsurface layer with densities between 25.0 and 26.5 σ_θ (Figure 4c). This subsurface plume water was characterized by cold

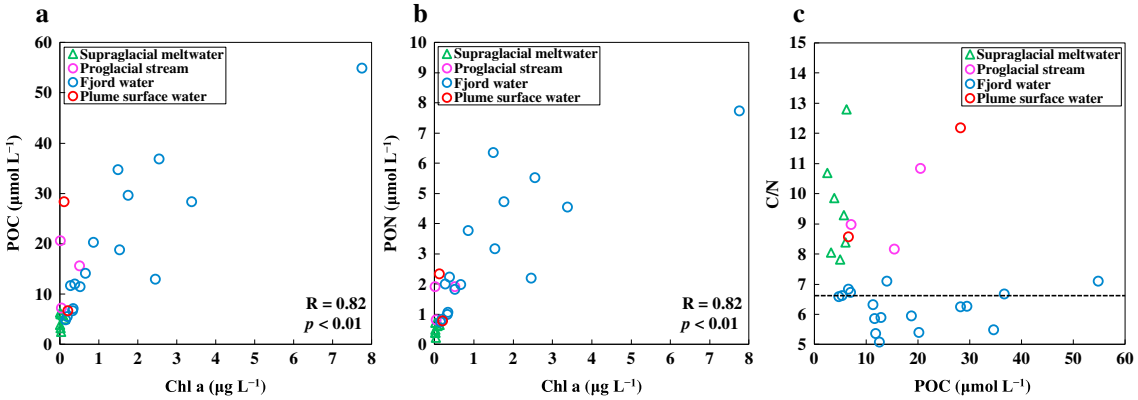

Figure 3. Relationships between concentrations of chlorophyll *a* (Chl *a*) and (a) particulate organic carbon (POC) and (b) particulate organic nitrogen (PON) in supraglacial meltwater, proglacial stream discharge, fjord water, and plume surface water. (c) Plots of carbon to nitrogen ratio versus POC concentration for these samples. The dotted line in (c) indicates the classical C/N ratio of 106:16, after Redfield et al. (1963).

temperature (<0.5°C) and high AOU (up to 72 μmol/kg; Figures 4a and 4d). Low-salinity (<31) and low-AOU (<70 μmol/kg) water (hereafter, fresh surface water) occurred near the surface with a density of <25.0 σ_θ (Figures 4b and 4d), and the highest Chl *a* concentration (up to 5.9 μg/L) was observed in this surface layer (Figure 4e).

The subsurface plume water extended off the calving front, and its turbidity progressively decreased toward the outer Bowdoin Fjord (Figures 5a, 5c, and 5d). The fresh surface water covered the entire fjord (Figure 5b). Chl *a* showed its maximum (up to 6.5 μg/L) near the boundary between the fresh surface water and subsurface plume water, and this Chl *a*-rich layer deepened toward the outer Bowdoin Fjord (Figure 5e).

Figure 7 shows the vertical distributions of the concentrations of macronutrients, DIC, and $\delta^{18}O$ values at the sampling sites along the centerline of the fjord. At stations situated within Bowdoin Fjord (Sts. D2–5), $NO_3^- + NO_2^-$ was depleted at the surface, whereas it was abundant deeper than 10 m (Figure 7a). At the station in the outer Bowdoin Fjord (St. D6), the $NO_3^- + NO_2^-$ concentration increased more gradually from the surface to the deeper layers (Figures 7a and 7f). Similar vertical distributions were observed for PO_4^{3-} and $Si(OH)_4$ (Figures 7b, 7c, 7g, and 7h). The concentrations of these macronutrients rapidly increased from the surface to the 10-m depth at Sts. D2–5, resulting in significantly higher concentrations at depths of 10–100 m compared with the values obtained at St. D6. It should be noted that the surface water at all stations contains only small amounts of $NO_3^- + NO_2^-$ and PO_4^{3-}. For $Si(OH)_4$, the concentration is significantly higher at Sts. D2–5 than at St. D6. DIC and $\delta^{18}O$ showed fairly uniform distributions over the sampling range, except for the significantly lower values obtained from the surface samples at Sts. D2–5 (Figures 7d, 7e, 7i, and 7j). However, the variation of $\delta^{18}O$ was small from the surface to the bottom at St. D6.

4. Discussion

4.1. Influence of Freshwater Discharge on Fjord Surface Water

Our data showed an apparent spatial gradient in the salinity of the fjord surface water, that is, salinity decreased as the sampling site approached the calving front (Figure 2c). Figure 8 shows the relationship between salinity and $\delta^{18}O$, which was obtained from all samples collected in the fjord and on the glacier. The water properties of the endmembers used in Figure 8 are listed in Table 2. The data lie around a mixing line between supraglacial meltwater and PW (GM-PW mixing line, connecting endmembers of GM and PW; Table 2), which explains the influence of glacial meltwater on the fjord water. The surface sample data deviate from the mixing line toward the upper left corner of the plot (Figure 8b), which suggests additional influences of sea-ice meltwater (e.g., $\delta^{18}O$ = 0.05 ± 2 in first-year sea ice from the Canadian Arctic

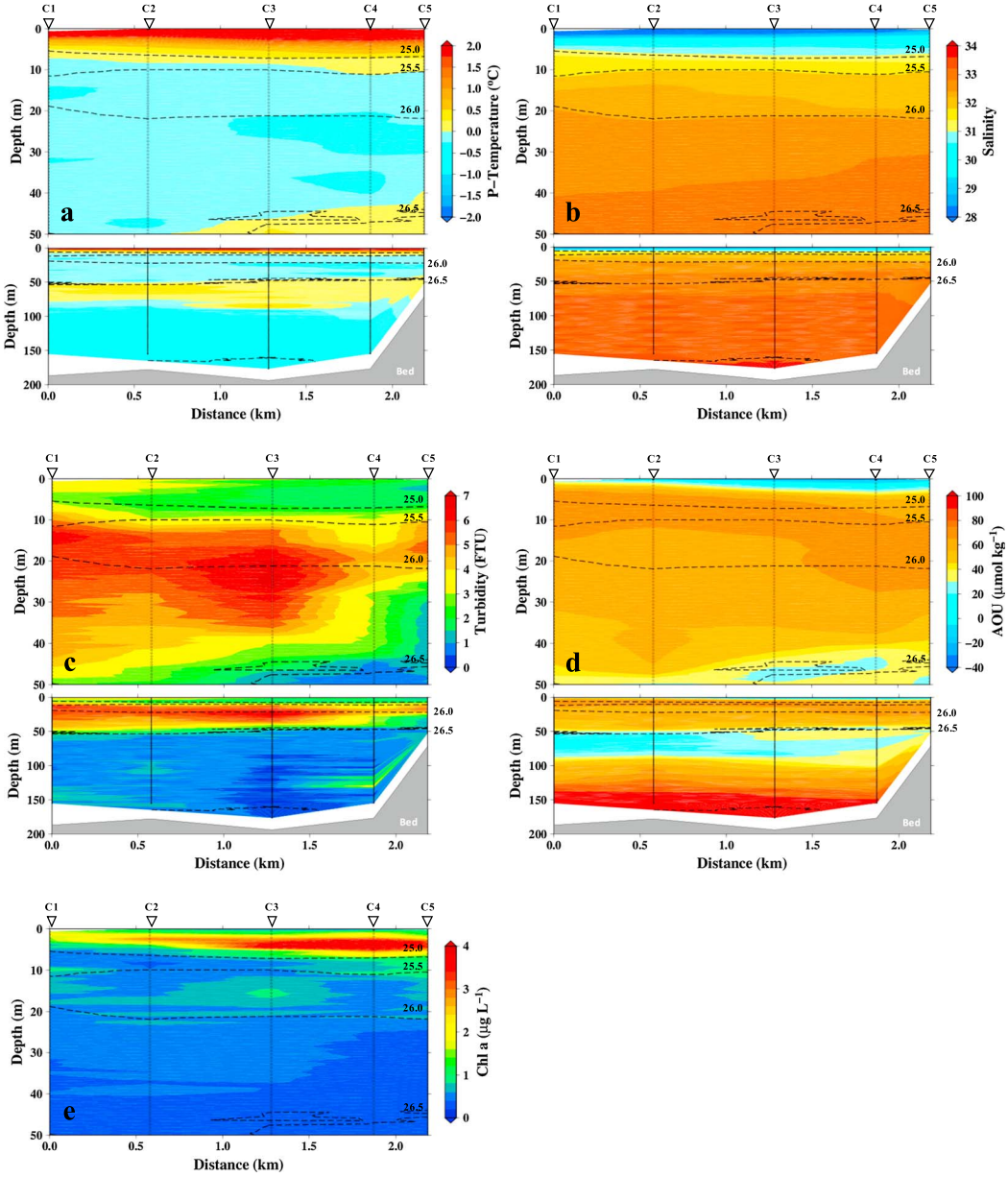

Figure 4. Water properties within a vertical cross section across Bowdoin Fjord 1.3 km from the calving front (Sts. C1–5 in Figure 1b), showing (a) potential temperature (P-Temperature), (b) salinity, (c) turbidity, and concentrations of (d) apparent oxygen utilization (AOU), and (e) chlorophyll *a* (Chl *a*). The vertical axis indicates water depth ranging from 0 to 50 m (upper panel) and from 0 to 200 m (lower panel, except for (e)). The horizontal axis indicates the eastward distance from St. C1. The dotted contours denote water density (σ_θ).

Archipelago and Baffin Bay; Alkire et al., 2010; Tan & Strain, 1980), as well as discharge from proglacial streams containing local snowmelt water with higher $\delta^{18}O$ values (e.g., $\delta^{18}O > -20‰$ in surface snow from a coastal area in northwestern Greenland in spring; Matoba et al., 2002). However, the data of the plume surface water deviates from the GM-PW mixing line toward the lower left corner of the plot (Figure 8b), which likely indicates the additional influences of fresh-water discharge with much lower $\delta^{18}O$ values from an efficient subglacial drainage system. Bhatia et al. (2011) have quantified the relative contributions of surface snow, glacial ice, and basal flow to the bulk subglacial discharge from a land-terminating southwestern Greenland glacier during the melt onset (May) and melt peak (July) periods. They defined the basal flow as water stored at the base of the glacier, which could consist of supraglacial waters stored at the base, basal-ice melt, and groundwater. The basal flow water comprised

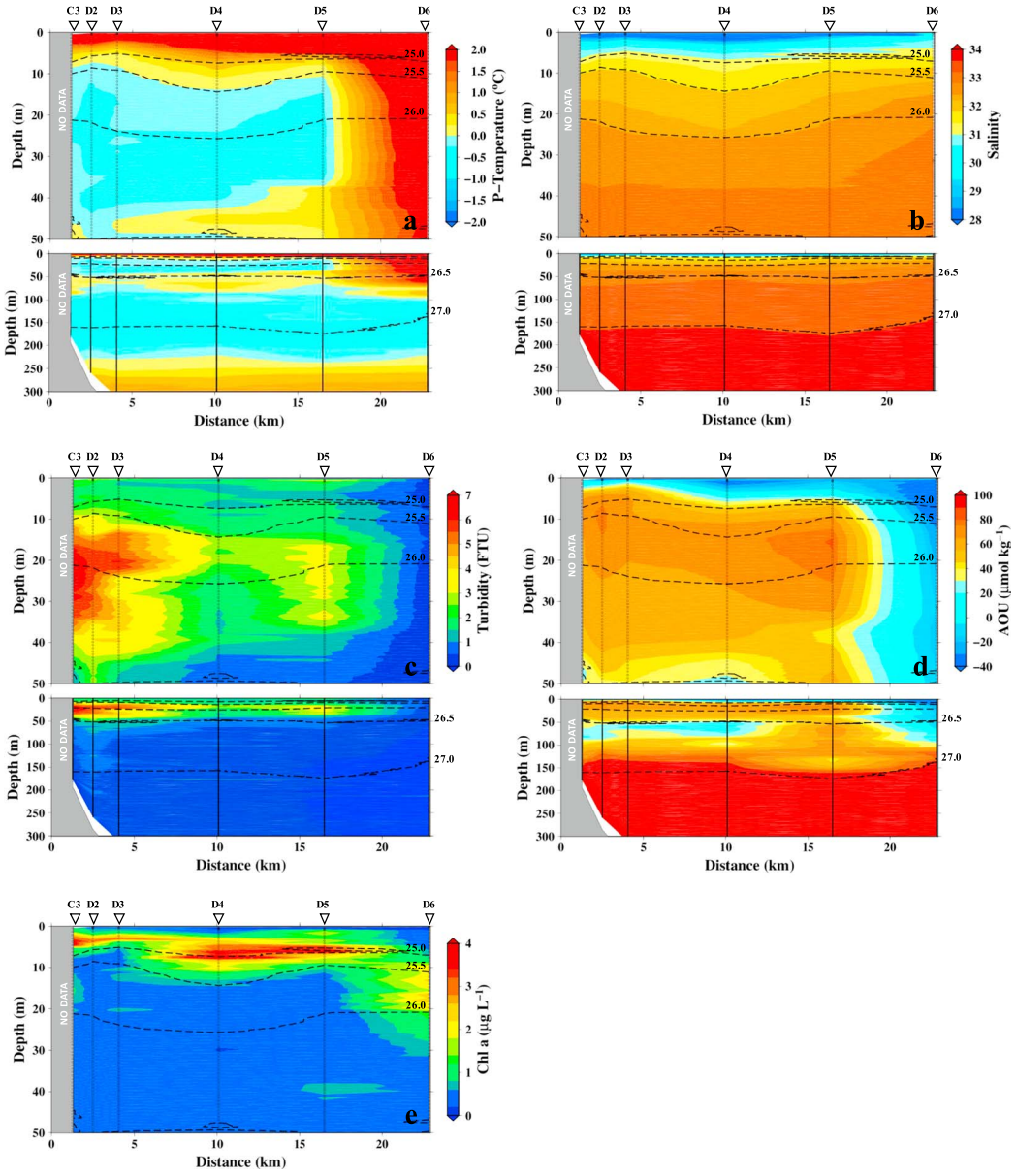

Figure 5. Water properties within a vertical cross section along the centerline of Bowdoin Fjord (Sts. C3 and D2–6 in Figure 1a), showing (a) potential temperature (P-Temperature), (b) salinity, (c) turbidity, and concentrations of (d) apparent oxygen utilization (AOU), and (e) chlorophyll *a* (Chl *a*). The vertical axis indicates water depth ranging from 0 to 50 m (upper panel) and from 0 to 300 m (lower panel, except for (e)). The horizontal axis indicates distance from the calving front. The dotted lines are contours of water density (σ_θ).

a greater fraction of the total discharge during May and was first diluted by snowmelt and then through increasing glacial ice melt as the season progressed. Applying this idea to our study area in northwestern Greenland, snow and glacial ice meltwater likely fed an efficient subglacial drainage system in mid-July. At a coastal site in the northwestern part of the Greenland Ice Sheet, the $\delta^{18}O$ of surface snow in late spring decreased from −22.2‰ to −38.4‰ with elevation (<1,230 m; Matoba et al., 2014). If we define the endmember of the lowest $\delta^{18}O$ value of snowmelt water to be −38.4‰, the plume surface water samples shown in Figure 8b are below the GM-PW mixing line but above the SM-PW line, which connects endmembers of SM and PW (Table 2). This result should be considered to explain the influence of snowmelt water discharge with notably low $\delta^{18}O$ value from up-glacier area, throughout a likely efficient subglacial drainage system on the plume, as well as the ambient glacial ice (and local snow) meltwater at our sampling site.

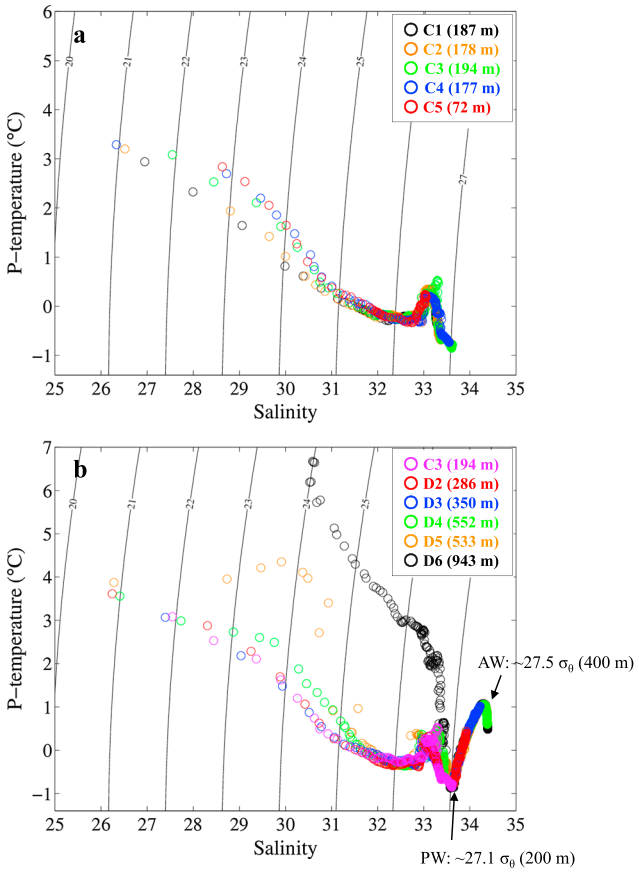

Figure 6. Potential temperature (P-Temperature) versus salinity along with isopycnals sampled within vertical cross sections (a) Sts. C1–5 and (b) Sts. C3 and D2–6. The ocean bottom water depth of each station is indicated in parentheses. Polar and Atlantic water are indicated as PW and AW (with water depths), respectively.

To quantify the fractions of freshwater in the plume surface water, we assume a simplified mixture of three components: supraglacial meltwater at our sampling site, snowmelt water originating from up-glacier area, and fjord water. Fractions of mass, salinity, and $\delta^{18}O$ balance equations are described using the water properties of these three endmembers (e.g., Østlund & Hut, 1984):

$$f_{GM} + f_{SM} + f_{PW} = 1, \quad (1)$$

$$f_{GM}{\cdot}S_{GM} + f_{SM}{\cdot}S_{SM} + f_{PW}{\cdot}S_{PW} = S_{obs}, \quad (2)$$

$$f_{GM}{\cdot}\delta_{GM} + f_{SM}{\cdot}\delta_{SM} + f_{PW}{\cdot}\delta_{PW} = \delta_{obs}, \quad (3)$$

where f, S, and δ are the fractions of mass, salinity, and $\delta^{18}O$ and the suffixes GM, SM, and PW indicate supraglacial meltwater, snowmelt water, and fjord water, respectively (Table 2). Because no measurement was performed for the snowmelt water originating from the up-glacier area in this study, previously reported values for surface snow at a coastal site in the northwestern part of the Greenland Ice Sheet (elevation <1,230 m) were used for S_{SM} and δ_{SM} (Matoba et al., 2014).

The mass fractions of these three water components computed by solving equations (1)–(3) are shown in Table 3. The waters influenced by the plume contain up to 14% of the ambient glacial ice (and local snow) meltwater at our sampling site and 5% of the snowmelt water originating from the up-glacier area, and the rest of the water is attributed to PW (as ambient fjord water) (Table 3). We interpret the results as indicating that these freshwaters upwell with significant amounts of deep PW, which results in substantially saline surface water within the plume more than in the other areas near the calving front (Figure 2c). The negative fraction obtained in the water influenced by the plume (Table 3) might be explained by the broad categories of end-member water sources; that is, $\delta^{18}O$ values between provenances in meltwaters such as englacial and subglacial meltwater should be considered (Bhatia et al., 2011; Yde & Knudsen, 2004; Yde et al., 2016). However, a crude estimate of the mass fraction in the plume showed that the deep PW accounted for >80% of the upwelling plume water.

4.2. Macronutrient Supply From Proglacial Streams

Although defining the freshwater endmember for this fjord is not straightforward in this study due to the limited number of surface runoff samples, we regarded the surface fjord water collected from highly turbid areas as proglacial stream discharge (indicated by blue and white arrows in Figure 2). Our data showed that supraglacial meltwater contained a small amount of macronutrients (Figure 2 and Table 1). Nevertheless, the surface fjord waters influenced by subglacial freshwater throughout the proglacial stream near Tugto Glacier were enriched in both $Si(OH)_4$ and PO_4^{3-} (Figures 2f and 2g). Satellite images shown in Figures 1a and 1b also indicate a turbid proglacial channel exiting Tugto Glacier from where it drains into the fjord (turbidity > 8 FTU) and where low salinity (<10) waters were observed (indicated by blue arrow in Figures 2a and 2c). The $Si(OH)_4$ and PO_4^{3-} concentrations in these areas were elevated to >13 and > 0.8 μmol/L, respectively, compared to the fjord waters at the furthest station D6, where the concentrations were <5 and <0.6 μmol/L in the top 100 m, respectively (Figures 7b, 7c, 7g, and 7h). According to previous studies, glacial meltwater becomes significantly enriched in dissolved solute (and nutrients) as it passes through the subglacial drainage system and entrains substantial quantities of reactive sediment generated by glacial physical erosion (Aciego et al., 2015; Hawkings et al., 2015; Yde et al., 2014). Evidence from previous studies in Greenland has shown that proglacial streams are enriched in dissolved and dissolvable amorphous silica, which is attributed to entrainment during rock weathering, and are the primary source of $Si(OH)_4$ into the surface of the fjord (Hawkings et al., 2015, 2017; Meire et al., 2016). Hawkings et al. (2016) have also reported that most dissolved P in glacial meltwaters is derived from the dissolution of P-containing rock. Elevated concentrations of $Si(OH)_4$ and PO_4^{3-} in the surface of the fjord near Tugto Glacier in this study

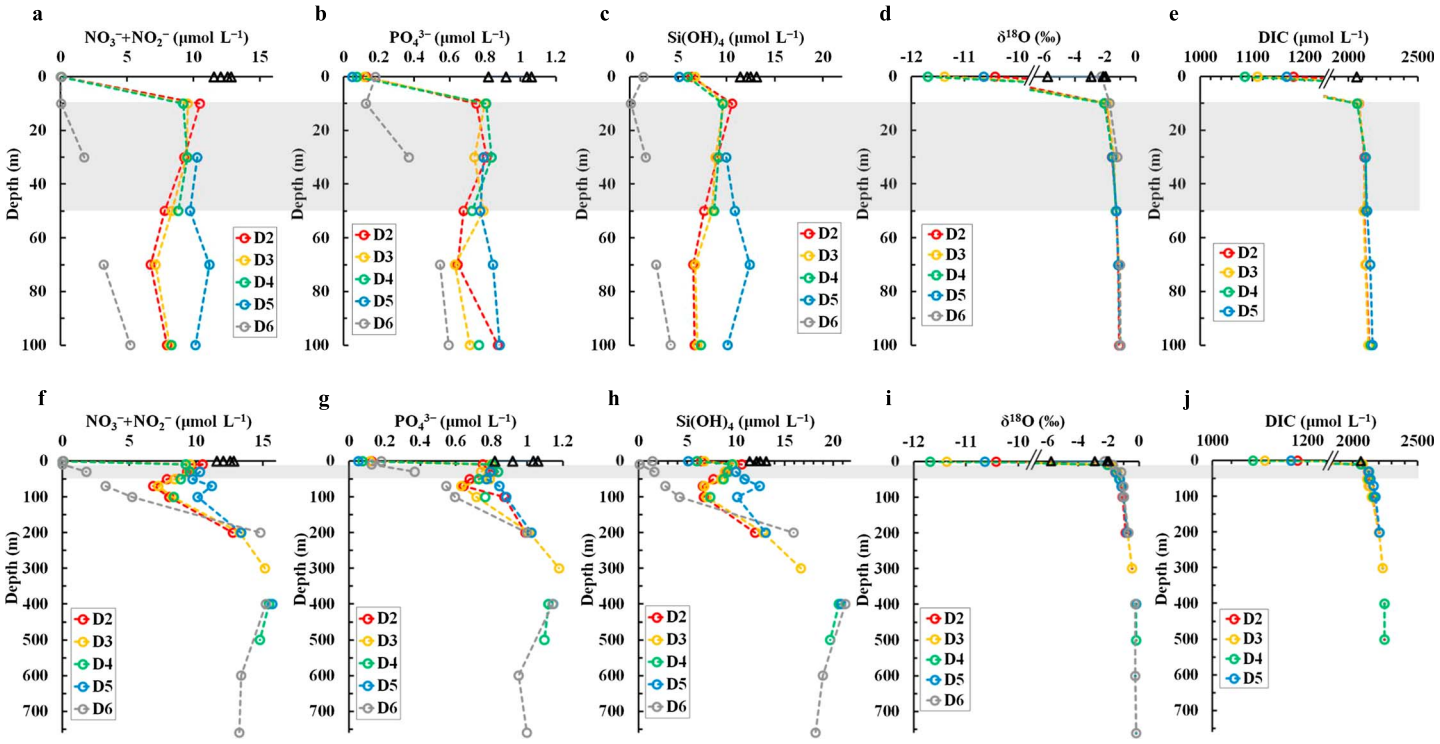

Figure 7. Vertical profiles of (a) NO_3^- + NO_2^-, (b) PO_4^{3-}, (c) $Si(OH)_4$, (d) $\delta^{18}O$, and (e) dissolved inorganic carbon (DIC) in the upper 100 m of Bowdoin Fjord. Data from the plume water samples are indicated by black triangles, and the depth range of subsurface plume water is indicated by gray shading. (f)–(j) The same data for the entire measurement depth.

are therefore likely to arise from glacial comminution of bedrock. There is likely to be some spatial variability in the geochemical composition of glacial meltwaters entering the fjord, due to varying geochemical and hydrological properties of ice sheet catchments. For instance, the large spatial variability in dissolved silica concentrations in glacial meltwaters is evident from data compilation in Meire et al. (2016). However, the NO_3^- + NO_2^- concentration was low in these areas (Figure 2e). This result suggests that the subglacial freshwater originating from Tugto Glacier is not a significant source of NO_3^- + NO_2^- likely causing a dilution of NO_3^- + NO_2^- in the fjord surface waters, which is potentially enhancing nitrogen limitation in the fjord. Upwelling by a subglacial freshwater driven

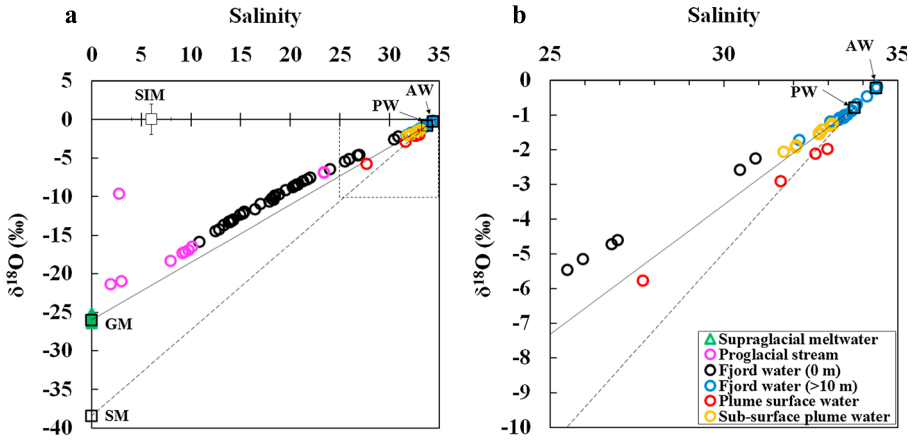

Figure 8. (a) $\delta^{18}O$ versus salinity in supraglacial meltwater, proglacial stream discharge, fjord water (0 and >10 m), and water influenced by plume. Squares denote endmembers of shown as supraglacial meltwater (GM), snowmelt water originating from up-glacier area (SM), sea-ice meltwater (SIM), polar water (PW), and Atlantic water (AW; see Table 2). The thick or dashed line is a mixing line, which connects PW with GM or SM, respectively. The box indicates the area shown in (b). The SM and SIM data are adopted from Matoba et al. (2014) and Alkire et al. (2010), respectively.

Table 2
Properties of Water Taken as Endmembers

Endmembers	Salinity (S_x)	$\delta^{18}O$ (δ_x)	N
Supraglacial meltwater (x = GM)	0	−26.0 ± 0.4	8
Snowmelt water (x = SM)	0	−38.4	—
Sea-ice meltwater (x = SIM)	6 ± 2	0.05 ± 2	—
Polar water (x = PW, 200 m)	33.8 ± 0.05	−0.78 ± 0.07	4
Atlantic water (x = AW, 400 m)	34.4 ± 0.01	−0.21 ± 0.02	3

Note. Salinity and $\delta^{18}O$ values of Polar and Atlantic waters are averaged values over the depth range of 200 and 400 m at Sts. D, respectively. Salinity and $\delta^{18}O$ values for snowmelt water originating from up-glacier area and sea-ice meltwater are adopted Matoba et al. (2014) and Alkire et al. (2010), respectively. *N* denotes the number of samples.

plume plays an important role in the $NO_3^- + NO_2^-$ supply to the surface and therefore generation of the high phytoplankton abundance, which is explained in sections 4.3 and 4.5.

4.3. Macronutrient Transport by the Subglacial Discharge Plume

Our data shown in Figures 4, 5, and 7 suggest that the vast majority of nutrients come from the upwelling plume. Above the subsurface plume water layer (Figures 4 and 5), a nutricline was observed between the depths of 0 and 10 m over the entire fjord (Figures 7a, 7b, and 7c). The nutricline was not formed in the outer Bowdoin Fjord, which is likely because it lies beyond the reach of the subsurface plume water. We interpret the nutricline formation within the fjord to be a result of discharge and upwelling of subglacial freshwater. Meire et al. (2016) have reported that the subglacial discharge plume in a fjord in southwest Greenland forms a supply route of macronutrients to the surface layer. This is because buoyant subglacial freshwater entrains a large volume of deep fjord water (Mortensen et al., 2013). Thus, we propose the following hypothesis: after being discharged into the ocean at the level of the glacier bed, subglacial freshwater upwells with nutrient-rich and high-AOU deep fjord water. The upwelled water reaches the surface and subducts to form the subsurface plume water below 10 m. This nutrient-rich layer is the reason why the nutrient concentration shows a steep gradient from the surface to 10 m. To verify this hypothesis, we analyzed the nutrient and AOU properties of the subsurface plume water and compared them with those of the deep fjord water.

According to Millero (2006), AOU is generally higher in denser water because of the biological use of oxygen for the respiration and oxidation of organic matter. $NO_3^- + NO_2^-$ and PO_4^{3-} are remineralized by the oxidation process, which results in higher $NO_3^- + NO_2^-$ and PO_4^{3-} concentrations in denser water. For silicate, however, part of its remineralization is not correlated with the biochemical oxidation of organic matter (Park, 1967). Figure 9 shows the relationships between macronutrient concentrations, turbidity, and AOU of our samples. The AOU at all stations of Bowdoin Fjord were linearly correlated with $NO_3^- + NO_2^-$ and PO_4^{3-}, which indicates that AOU was related to nutrient remineralization as the water became denser (Figures 9a and 9b). In contrast, it was related to consumption of the nutrient by the primary producer (associated with oxygen production) as water became lighter. The AOU and $Si(OH)_4$ have a weaker linear relationship compared to $NO_3^- + NO_2^-$ and PO_4^{3-}, which could be attributed to significant $Si(OH)_4$ added to the lighter water ($<25.0\ \sigma_\theta$) over the inner Bowdoin Fjord by the sediment-laden meltwaters from nearby land-terminating glaciers (Figures 9c and 9d).

Our observations in the outer Bowdoin Fjord are consistent with the above theory described by Millero (2006) because AOU, $NO_3^- + NO_2^-$, and PO_4^{3-} increase as the water becomes denser in outer Bowdoin Fjord (St. D6 [stars] in Figures 9a and 9b). However, water in the inner Bowdoin Fjord showed a different feature. Water within a relatively large density range of 25.0–27.0 σ_θ showed similar properties, that is, AOU = ~29–75 μmol/kg, $NO_3^- + NO_2^-$ = ~7–11 μmol/L, and PO_4^{3-} = ~0.6–0.9 μmol/L (Sts. D2–5 [blue, light blue, yellow, and light orange dots] in Figures 9a and 9b). The subsurface plume water lies within this density range (25.0–26.5 σ_θ; Figure 9d). If we compare waters with the same density, AOU, $NO_3^- + NO_2^-$, and PO_4^{3-} concentrations in the subsurface plume water are significantly higher than those at St. D6. This water is less dense (25.0 to 26.5 σ_θ) than PW (~27.1 σ_θ) because it is diluted with subglacial freshwater, but the water maintains relatively similar properties as PW, which shows relatively nutrient-rich and high-AOU. The nutrient enrichment of the subsurface plume water from the subglacial discharge is apparently not significant because the relations between AOU and $NO_3^- + NO_2^-$ and PO_4^{3-} (also a part of $Si(OH)_4$) concentrations in the subsurface plume water (within 25.0–26.5 σ_θ, which is shown by blue and light blue dots in Figures 9a, 9b, and 9c) do not considerably deviate from linear relationships. Accordingly, water in the inner Bowdoin Fjord with densities between 25.0 and 27.0 σ_θ

Table 3
Estimated Mass Fractions of Supraglacial Meltwater (f_{GM}), Snowmelt Water Originating From Up-Glacier Area (f_{SM}), and Polar Water in Water Influenced by Plume (f_{PW})

Samples	f_{GM}	f_{SM}	f_{PW}	N
Plume surface water (0 m)	−0.03 to 0.14	0.04 to 0.05	0.82 to 0.98	4
Subsurface plume water (10–50 m)	0.01 to 0.08	−0.02 to 0	0.94 to 0.98	11

Note. N denotes the number of samples.

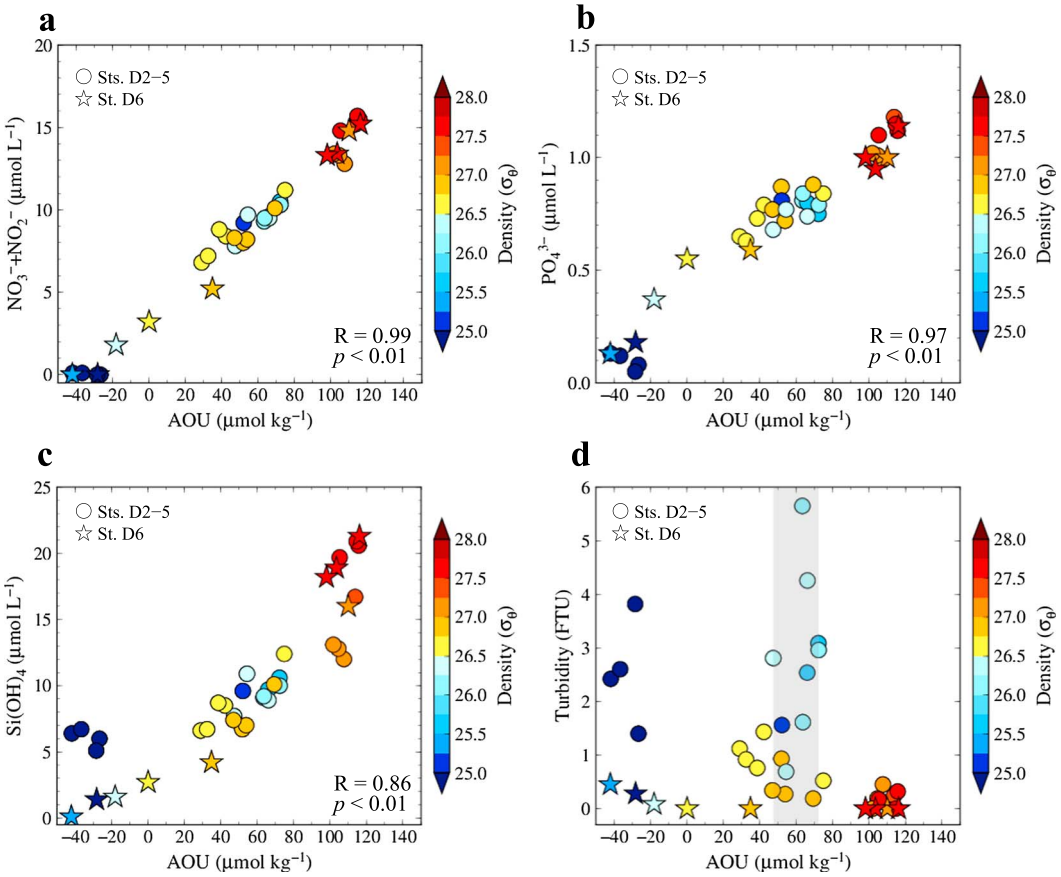

Figure 9. Apparent oxygen utilization (AOU) versus (a) $NO_3^- + NO_2^-$, (b) PO_4^{3-}, (c) $Si(OH)_4$, and (d) turbidity in the inner (Sts. D2–5; dots) and outer (St. D6; stars) Bowdoin Fjord. The color scale indicates the seawater density. The linear relationships of AOU with $NO_3^- + NO_2^-$, PO_4^{3-}, and $Si(OH)_4$ were evaluated by Pearson correlation coefficients (*R*). The AOU range of subsurface plume water in the inner Bowdoin Fjord is indicated by gray shading in (d).

show similar properties, which results from the modification of PW by subglacial freshwater and the subsequent formation of subsurface plume water (Figures 9 and 10). The foregoing analysis indicates that upwelling of subglacial freshwater plays a dominant role in the vertical transport of macronutrients, especially for $NO_3^- + NO_2^-$ and PO_4^{3-}, from the deeper region to the fjord surface.

The entrainment of nutrient-rich deep water into the plume was also confirmed by the sampling of plume surface water from the calving front (St. P, Figure 1). During our field activities on the glacier (4–21 July 2016), the surface water current was pushing sea ice off the calving front, and a round, ice-free zone was consistently present. This observation indicates that the forced convection associated with the buoyant plume reached the surface. The salinity of the plume surface water was notably higher than that of the water sampled outside of the plume (Table 1), which implies upwelling of high salinity deep water, which was reported for the other glaciated fjords in Greenland (Bendtsen et al., 2015; Mankoff et al., 2016; Meire et al., 2017). The concentrations of macronutrients in the plume surface water were notably higher than those outside of the plume (Table 1). For example, the $NO_3^- + NO_2^-$ concentration of the plume surface water was 12.3 ± 0.6 μmol/L, whereas it was close to the detection limit (0.2 ± 0.2 μmol/L) outside the plume. The concentration of Chl *a* was significantly low in the plume (0.1 ± 0.1 μg/L), which is presumably due to a low abundance of phytoplankton in the upwelled water. The relatively high-$\delta^{18}O$ observed in the plume surface water (−3.2 ± 1.8‰) also indicates a large amount of PW entrainment into the plume. Based on the calculation described in section 4.1, the fraction of supraglacial meltwater (f_{GM}) in the plume surface water was estimated to be ~0.14. This fraction is consistent with the value previously estimated from temperature and salinity measurements in glaciated fjords in Greenland, which is ~0.1 (Bendtsen et al., 2015; Mankoff et al., 2016; Mortensen et al., 2013).

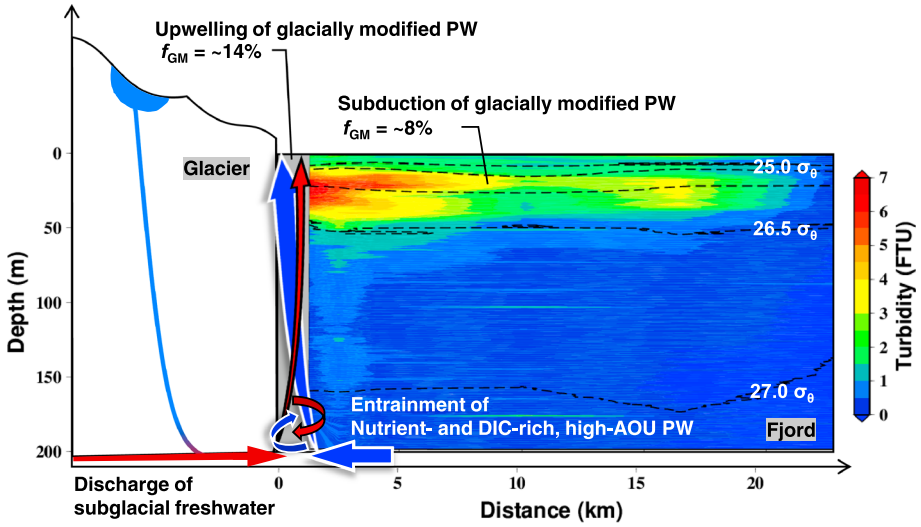

Figure 10. Schematic of the nutrient-rich and high apparent oxygen utilization (AOU) subsurface plume water formation at the front of Bowdoin Glacier. f_{GM} is the fraction of supraglacial meltwater described in the text. PW indicates polar water with a density of ~27.1 σ_θ. DIC = dissolved inorganic carbon.

To quantify the contribution of the plume to macronutrient transport, we estimated the amount of $NO_3^- + NO_2^-$ transported to the fjord surface by the plume. The plume water flux, Q_{plu}, was estimated by the following equation (Mankoff et al., 2016):

$$Q_{plu} = v_{plu} \cdot A_{plu} \quad (4)$$

where v_{plu} is the plume water current velocity off the glacier and A_{plu} is the vertical sectional area of the plume that is parallel to the calving front (Mankoff et al., 2016). Thus, the actual Q_{plu} was calculated as the horizontal transport of the plume, and we assumed that it is equivalent to vertical transport. Because v_{plu} was unavailable in this study, we assumed a value of 0.84 m/s, which was obtained following direct measurements in the upper 20 m of the fjord in front of a midsized marine-terminating outlet glacier in Greenland (see Figure 10 in Mankoff et al., 2016). The plume width at the surface was approximately 100 m according to a Landsat 8 satellite image, which was acquired on 14 July 2016. The maximum depth of the plume was set to 40 m based on the thickness of the subsurface plume water layer at depths of 10–50 m (Figures 4c and 5c). We assumed an inverted triangle as the cross section of the plume such that A_{plu} was approximated as 2,000 m^2 (A_{plu} = 40 m × 100 m × 0.5; Figure S2). These values provide an estimated Q_{plu} value of 1,680 m^3/s. The flux of $NO_3^- + NO_2^-$ transported by the plume, $F(N + N)_{plu}$, is calculated from the $NO_3^- + NO_2^-$ concentration $C(N + N)_{plu}$.

$$F(N+N)_{plu} = Q_{plu} \times C(N+N)_{plu} \quad (5)$$

Using the mean $NO_3^- + NO_2^-$ concentration in the plume surface water (12.3 μmol/L, Table 1), we obtained $F(N + N)_{plu}$ = 21 mol/s. Following the same procedure, we obtained the fluxes of PO_4^{3-}, $Si(OH)_4$, and DIC transported by the plume as 1.7, 21, and 3.5 × 10^3 mol/s, respectively. These values indicate the importance of the plume in macronutrient and DIC transport to near the surface waters in front of Bowdoin Glacier.

4.4. Particle Transport by the Subglacial Discharge Plume

The SS concentration inside the plume was several times greater than the concentrations obtained outside of the plume (Table 1). Organic carbon and nitrogen ratios (C/N ratios) in the fjord water were similar to those commonly reported for biogenic substances produced by phytoplankton (e.g., C/N [mol/mol] = 6.9–7.6 in spring surface water in a fjord in Svalbard [Svendsen et al., 2002] and 6.1 ± 0.8 in the mixed-layer of seawater during the productive season in the northeast Atlantic Ocean [Körtzinger et al., 2001]; Figure 3c). However, C/N ratios of the plume surface water, as well as supraglacial meltwater and proglacial stream discharge, were greater than those in the ambient fjord water (Figure 3c). Thus, the particles generated from the flushing of

stored waters in the subglacial environment showed nitrogen-depleting conditions regardless of the POC concentration. According to Lawson et al. (2014), POC derived from the ice sheet bed via the erosion of bedrock and overridden paleosols contains a significant bioreactive component (extractable carbohydrates), which is potentially bioavailable. Additionally, reactive particulate material originating from glacial meltwaters discharges into the fjord (Hawkings et al., 2017). This material potentially plays an important role in the supply of dissolved silica, which may provide conditions favorable for diatom growth over other phytoplankton species further down fjord.

4.5. Effect of $NO_3^- + NO_2^-$ Supply Via Subsurface Plume Water on Phytoplankton Growth

Our data showed a high abundance of phytoplankton (~6.5 μg/L Chl *a*) near the boundary between the relatively fresh surface water and subsurface plume water in the inner Bowdoin Fjord (Figure 5e). To quantify the importance of horizontal transport of plume water on the distribution of phytoplankton in a glaciated fjord, we computed the vertical gradient in the $NO_3^- + NO_2^-$ concentration in the nitracline $\partial(NO_3^- + NO_2^-)/\partial z$ (mmol/m^4) at depths of 0–10 m for Sts. D2–4 and 10–200 m for St. D6, respectively (Figure 7). The vertical gradient is an important parameter to determine the vertical flux of $NO_3^- + NO_2^-$ from the subsurface to the surface layers. The estimated vertical gradient was an order of magnitude greater in the inner (0.92–1.04 mmol/m^4, Sts. D2–4) than in the outer (0.08 mmol/m^4, St. D6) Bowdoin Fjord. Since the subduction of plume water transports high $NO_3^- + NO_2^-$ water to the subsurface layer (Figures 4, 5, and 7), the strong vertical gradient should be formed in the inner fjord. Our results suggest that the vertical flux of $NO_3^- + NO_2^-$ near the surface is enhanced by the strong gradient of $NO_3^- + NO_2^-$, which is likely associated with high abundance of phytoplankton. Moreover, the Chl *a* concentration was lower in the outer Bowdoin Fjord at St. D6, which was presumably due to a $NO_3^- + NO_2^-$ limitation at a depth of 10 m because a Chl *a*-rich water layer occurred at greater depths (Figures 5e and 7a). We also observed highly turbid and Chl *a*-rich surface water at 77°33′N in the fjord (Figures 2a and 2i), which was influenced by meltwater input from sediment-laden stream to the west (satellite imagery in Figure 1a). The supply of nitrogen to these Chl *a*-rich waters likely occurred from below the surface, not from meltwater input, as described in section 4.2.

5. Conclusions

To better understand the influence of subglacial freshwater discharge and plume formation on nutrient and DIC transport in a fjord, we performed oceanographic measurements and water sampling in Bowdoin Fjord and on Bowdoin Glacier in northwestern Greenland. $NO_3^- + NO_2^-$ concentrations from supraglacial meltwaters indicate that local glaciers may not be an important source of nitrogen in the fjord. The concentrations of macronutrients and DIC in the plume surface water were several times greater than those sampled outside of the plume. Salinity and SS concentrations were notably higher in the plume surface water, which suggests upwelling of saline deep water. The upwelled water was highly turbid because it contained a substantial amount of subglacial sediments.

Upwelling of nutrient-rich deep water was also confirmed by the AOU in the fjord water, as well as the freshwater fractions in the plume surface water, which were computed based on $\delta^{18}O$ values. Our data demonstrate that deep fjord water was entrained in the subglacial discharge and transported as plume water to the surface or subsurface of the fjord (Figure 10). Turbid subsurface plume water was observed in a subsurface layer with densities between 25.0 and 26.5 σ_θ. Phytoplankton blooms were observed near the boundary between the fresh surface water and subsurface plume water layers. The bloom was associated with a strong upward $NO_3^- + NO_2^-$ flux, which was caused by the subduction of the plume water. Our study results show that subglacial freshwater discharge plays a key role in the availability of nutrients and the subsequent growth of phytoplankton in Bowdoin Fjord.

Acknowledgments
We thank the members of the 2016 field campaign in Qaanaaq. Special thanks are due to S. Daorana, T. Oshima, and K. Peterson for providing logistic support in Qaanaaq. We are grateful to J. Nishioka, S. Aoki, O. Seki, and K. Ono for assistance with the laboratory work. The authors wish to acknowledge J. Nishioka, S. Matoba, and Y. Matsumura for helpful comments on the manuscript. Some observational equipment was constructed by the workshop of the Institute of Low Temperature Science, Hokkaido University. This research was funded by MEXT (Japanese Ministry of Education, Culture, Sports, Science and Technology) through the Arctic research project Arctic Challenge for Sustainability (ArCS). This research was also supported by the Grant for Joint Research Program of the Institute of Low Temperature Science, Hokkaido University. Finally, we would like to thank Miguel Goni and two anonymous reviewers for their constructive comments. Data used in this study are available in the supporting information (Figures S1 and S2 and Datasets S1 and S2).

References

Aciego, S. M., Stevenson, E. I., & Arendt, C. A. (2015). Climate versus geological controls on glacial meltwater micronutrient production in southern Greenland. *Earth and Planetary Science Letters*, *424*, 51–58. https://doi.org/10.1016/j.epsl.2015.05.017

Alkire, M. B., Falkner, K. K., Boyd, T., & Macdonald, R. W. (2010). Sea ice melt and meteoric water distributions in Nares Strait, Baffin Bay, and the Canadian Arctic Archipelago. *Journal of Marine Research*, *68*(6), 767–798. https://doi.org/10.1357/002224010796673867

Beaird, N., Straneo, F., & Jenkins, W. (2015). Spreading of Greenland meltwaters in the ocean revealed by noble gases. *Geophysical Research Letters*, *42*, 7705–7713. https://doi.org/10.1002/2015GL065003

Bendtsen, J., Mortensen, J., Lennert, K., & Rysgaard, S. (2015). Heat sources for glacial ice melt in a west Greenland tidewater outlet glacier fjord: The role of subglacial freshwater discharge. *Geophysical Research Letters*, *42*, 4089–4095. https://doi.org/10.1002/2015GL063846

Benson, B. B., & Krause, D. (1984). The concentration and isotopic fractionation of oxygen dissolved in freshwater and seawater in equilibrium with the atmosphere. *Limnology and Oceanography*, *29*(3), 620–632. https://doi.org/10.4319/lo.1984.29.3.0620

Bhatia, M. P., Das, S. B., Kujawinski, E. B., Henderson, P., Burke, A., & Charette, M. A. (2011). Seasonal evolution of water contributions to discharge from a Greenland outlet glacier: Insight from a new isotope-mixing model. *Journal of Glaciology*, *57*(205), 929–941. https://doi.org/10.3189/002214311798043861

Chu, V. W. (2014). Greenland ice sheet hydrology. *Progress in Physical Geography*, *38*(1), 19–54. https://doi.org/10.1177/0309133313507075

Chu, V. W., Smith, L. C., Rennermalm, A. K., Forster, R. R., & Box, J. E. (2012). Hydrologic controls on coastal suspended sediment plumes around the Greenland Ice Sheet. *The Cryosphere*, *6*(1), 1–19. https://doi.org/10.5194/tc-6-1-2012

Fransson, A., Chierici, M., Nomura, D., Granskog, M. A., Kristiansen, S., Martma, T., & Nehrke, G. (2015). Effect of glacial drainage water on the CO_2 system and ocean acidification state in an Arctic tidewater-glacier fjord during two contrasting years. *Journal of Geophysical Research: Oceans*, *120*, 2413–2429. https://doi.org/10.1002/2014JC010320

Gardner, A. S., Moholdt, G., Cogley, J. G., Wouters, B., Arendt, A. A., Wahr, J., et al. (2013). A reconciled estimate of glacier contributions to sea level rise: 2003 to 2009. *Science*, *340*(6134), 852–857. https://doi.org/10.1126/science.1234532

Hawkings, J., Wadham, J. L., Benning, L. G., Hendry, K. R., Tranter, M., Tedstone, A., et al. (2017). Ice sheets as a missing source of silica to the polar oceans. *Nature Communications*, *8*, 14198. https://doi.org/10.1038/ncomms14198

Hawkings, J., Wadham, J. L., Tranter, M., Telling, J., Bagshaw, E., Beaton, A., et al. (2016). The Greenland Ice Sheet as a hot spot of phosphorus weathering and export in the Arctic. *Global Biogeochemical Cycles*, *30*, 191–210. https://doi.org/10.1002/2015GB005237

Hawkings, J. R., Wadham, J. L., Tranter, M., Lawson, E., Sole, A., Cowton, T., et al. (2015). The effect of warming climate on nutrient and solute export from the Greenland Ice Sheet. *Geochemical Perspectives Letters*, *1*, 94–104.

Hopwood, M. J., Bacon, S., Arendt, K., Connelly, D. P., & Statham, P. J. (2015). Glacial meltwater from Greenland is not likely to be an important source of Fe to the North Atlantic. *Biogeochemistry*, *124*, 1–11.

Hopwood, M. J., Connelly, D. P., Arendt, E. K., Juul-Pedersen, T., Stinchcombe, M. C., Meire, L., et al. (2016). Seasonal changes in Fe along a glaciated Greenlandic fjord. *Frontiers in Earth Science*, *4*, 15. https://doi.org/10.3389/feart.2016.00015

Johnson, K. M., King, A. E., & Sieburth, J. M. (1985). Coulometric TCO_2 analyses for marine studies: An introduction. *Marine Chemistry*, *16*(1), 61–82. https://doi.org/10.1016/0304-4203(85)90028-3

Kattner, G. (1999). Storage of dissolved inorganic nutrients in seawater: Poisoning with mercuric chloride. *Marine Chemistry*, *67*(1-2), 61–66. https://doi.org/10.1016/S0304-4203(99)00049-3

Körtzinger, A., Koeve, W., Kähler, P., & Mintrop, L. (2001). C:N ratios in the mixed layer during the productive season in the northeast Atlantic Ocean. *Deep Sea Research, Part I*, *48*(3), 661–688. https://doi.org/10.1016/S0967-0637(00)00051-0

Lawson, E. C., Wadham, J. L., Tranter, M., Stibal, M., Lis, G. P., Butler, C. E. H., et al. (2014). Greenland Ice Sheet exports labile organic carbon to the Arctic oceans. *Biogeosciences*, *11*(14), 4015–4028. https://doi.org/10.5194/bg-11-4015-2014

Lydersen, C., Assmy, P., Falk-Petersen, S., Kohler, J., Kovacs, K. M., Reigstad, M., et al. (2014). The importance of tidewater glaciers for marine mammals and seabirds in Svalbard, Norway. *Journal of Marine Systems*, *129*, 452–471. https://doi.org/10.1016/j.jmarsys.2013.09.006

Mankoff, K. D., Straneo, F., Cenedese, C., Das, S. B., Richards, C. G., & Singh, H. (2016). Structure and dynamics of a subglacial discharge plume in a Greenlandic fjord. *Journal of Geophysical Research: Oceans*, *121*, 8670–8688. https://doi.org/10.1002/2016JC011764

Matoba, S., Yamasaki, T., Miyahara, M., & Motoyama, H. (2014). Spatial variations of $\delta^{18}O$ and ion species in the snowpack of the northwestern Greenland ice sheet. *Bulletin of Glaciological Research*, *32*, 79–84. https://doi.org/10.5331/bgr.32.79

Matoba, S., Yamasaki, T., & Motoyama, H. (2002). Meteorological observation and chemical compositions of precipitation during the winter and spring season in 1997/98 at Siorapaluk, northwetern Greenland. *Bulletin of Glaciological Research*, *19*, 25–31.

Meire, L., Meire, P., Struyf, E., Krawczyk, D. W., Arendt, K. E., Yde, J. C., et al. (2016). High export of dissolved silica from the Greenland Ice Sheet. *Geophysical Research Letters*, *43*(17), 9173–9182. https://doi.org/10.1002/2016GL070191

Meire, L., Mortensen, J., Meire, P., Juul-Pedersen, T., Sejr, M. K., Rysgaard, S., et al. (2017). Marine-terminating glaciers sustain high productivity in Greenland fjords. *Global Change Biology*, *23*(12), 5344–5357. https://doi.org/10.1111/gcb.13801

Millero, F. J. (2006). Dissolved gases other than CO_2. In *Chemical oceanography*, (3rd ed.pp. 211–240). Boca Raton: Taylor & Francis.

Mortensen, J., Bendtsen, J., Motyka, R. J., Lennert, K., Truffer, M., Fahnestock, M., & Rysgaard, S. (2013). On the seasonal freshwater stratification in the proximity of fast-flowing tidewater outlet glaciers in a sub-Arctic sill fjord. *Journal of Geophysical Research: Oceans*, *118*, 1382–1395. https://doi.org/10.1002/jgrc.20134

Ohashi, Y., Iida, T., Sugiyama, S., & Aoki, S. (2016). Spatial and temporal variations in high turbidity surface water off the Thule region, northwestern Greenland. *Polar Science*, *10*(3), 270–277. https://doi.org/10.1016/j.polar.2016.07.003

Østlund, H. G., & Hut, G. (1984). Arctic Ocean water mass balance from isotope data. *Journal of Geophysical Research*, *89*(C4), 6373–6381. https://doi.org/10.1029/JC089iC04p06373

Overeem, I., Hudson, B. D., M, J. P., Syvitski, A. B., Mikkelsen, B., Hasholt, M. R., et al. (2017). Substantial export of suspended sediment to the global oceans from glacial erosion in Greenland. *Nature Geoscience*, *10*(11), 859–863. https://doi.org/10.1038/ngeo3046

Park, K. (1967). Nutrient regeneration and preformed nutrients off Oregon. *Limnology and Oceanography*, *12*(2), 353–357. https://doi.org/10.4319/lo.1967.12.2.0353

Redfield, A. C., Ketchum, B. H., & Richards, F. A. (1963). The influence of organisms on the composition of sea-water. In M. N. Hill (Ed.), *The sea* (Vol. 2, pp. 26–77). New York: Interscience.

Straneo, F., Sutherland, D. A., Holland, D., Gladish, C., Hamilton, G. S., Johnson, H. L., et al. (2012). Characteristics of ocean waters reaching Greenland's glaciers. *Annals of Glaciology*, *53*(60), 202–210. https://doi.org/10.3189/2012AoG60A059

Sugiyama, S., Sakakibara, D., Tsutaki, S., Maruyama, M., & Sawagaki, T. (2015). Glacier dynamics near the calving front of Bowdoin Glacier, northwestern Greenland. *Journal of Glaciology*, *61*(226), 223–232. https://doi.org/10.3189/2015JoG14J127

Suzuki, R., & Ishimaru, T. (1990). An improved method for the determination of phytoplankton chlorophyll using *N*,*N*-dimethylformamide. *Journal of Oceanography*, *46*, 190–194.

Svendsen, H., Beszczynska-Møller, A., Hagen, J. O., Lefauconnier, B., Tverberg, V., Gerland, S., et al. (2002). The physical environment of Kongsfjorden–Krossfjorden, an Arctic fjord system in Svalbard. *Polar Research*, *21*(1), 133–166.

Tan, F. C., & Strain, P. M. (1980). The distribution of sea ice meltwater in the eastern Canadian Arctic. *Journal of Geophysical Research*, *85*(C4), 1925–1932. https://doi.org/10.1029/JC085iC04p01925

Tsutaki, S., Sugiyama, S., Sakakibara, D., & Sawagaki, T. (2016). Surface elevation changes during 2007–13 on Bowdoin and Tugto Glaciers, northwestern Greenland. *Journal of Glaciology*, *62*(236), 1083–1092. https://doi.org/10.1017/jog.2016.106

Urbanski, J. A., Stempniewicz, L., Węsławski, J. M., Dragańska-Deja, K., Wochna, A., Goc, M., & Iliszko, L. (2017). Subglacial discharges create fluctuating foraging hotspots for sea birds in tidewater glacier bays. *Scientific Reports*, *7*, 43999. https://doi.org/10.1038/srep43999

Wadham, J. L., Hawkings, J., Telling, J., Chandler, D., Alcock, J., Lawson, E., et al. (2016). Sources, cycling and export of nitrogen on the Greenland Ice Sheet. *Biogeosciences*, *13*(22), 6339–6352. https://doi.org/10.5194/bg-13-6339-2016

Welshmeyer, N. A. (1994). Fluorometric analysis of chlorophyll *a* in the presence chlorophyll *b* and phaeopigments. *Limnology and Oceanography*, *39*(8), 1985–1992. https://doi.org/10.4319/lo.1994.39.8.1985

Yde, J. C., & Knudsen, N. T. (2004). The importance of oxygen isotope provenance in relation to solute content of bulk meltwaters at Imersuaq Glacier, West Greenland. *Hydrological Processes*, *18*(1), 125–139. https://doi.org/10.1002/hyp.1317

Yde, J. C., Knudsen, N. T., Hasholt, B., & Mikkelsen, A. B. (2014). Meltwater chemistry and solute export from a Greenland Ice Sheet catchment, Watson River, West Greenland. *Journal of Hydrology*, *519*, 2165–2179. https://doi.org/10.1016/j.jhydrol.2014.10.018

Yde, J. C., Knudsen, N. T., Steffensen, J. P., Carrivick, J. L., Hasholt, B., Ingeman-Nielsen, T., et al. (2016). Stable oxygen isotope variability in two contrasting glacier river catchments in Greenland. *Hydrology and Earth System Sciences*, *20*(3), 1197–1210. https://doi.org/10.5194/hess-20-1197-2016